

Article

Silver Nanoparticles Grown on Cross-Linked Poly (Methacrylic Acid) Microspheres: Synthesis, Characterization, and Antifungal Activity Evaluation

Panagiotis Kainourgios ¹, Leto-Aikaterini Tziveleka ², Ioannis A. Kartsonakis ¹, Efstathia Ioannou ²,
Vassilios Roussis ² and Costas A. Charitidis ^{1,*}

¹ Research Unit of Advanced, Composite, Nano-Materials and Nanotechnology, School of Chemical Engineering, National Technical University of Athens, 9 Heroon Polytechniou St., Zographos, GR-15773 Athens, Greece; pkainourgios@chemeng.ntua.gr (P.K.); ikartso@chemeng.ntua.gr (I.A.K.)

² Section of Pharmacognosy and Chemistry of Natural Products, Department of Pharmacy, National and Kapodistrian University of Athens, Panepistimiopolis Zografou, GR-15771 Athens, Greece; ltziveleka@pharm.uoa.gr (L.-A.T.); eioannou@pharm.uoa.gr (E.I.); roussis@pharm.uoa.gr (V.R.)

* Correspondence: charitidis@chemeng.ntua.gr; Tel.: +30-21-0772-4046

Abstract: Silver nanoparticles (AgNPs) exert profound physicochemical, biological, and antimicrobial properties, therefore, they have been extensively studied for a variety of applications such as food packaging and cultural heritage protection. However, restrictions in their stability, aggregation phenomena, and toxicity limit their extensive use. Hence, the use of functional substrates that promote the silver nanoparticles' growth and allow the formation of uniform-sized, evenly distributed, as well as stable nanoparticles, has been suggested. This study reports on the fabrication and the characterization of hydrophilic polymer spheres including nanoparticles with intrinsic antifungal properties. Poly (methacrylic acid) microspheres were synthesized, employing the distillation precipitation method, to provide monodisperse spherical substrates for the growth of silver nanoparticles, utilizing the co-precipitation of silver nitrate in aqueous media. The growth and the aggregation potential of the silver nanoparticles were studied, whereas the antifungal activity of the produced nanostructures was evaluated against the black mold-causing fungus *Aspergillus niger*. The produced structures exhibit dose-dependent antifungal activity. Therefore, they could potentially be employed for the protection and preservation of cultural heritage artifacts and considered as new agents for food protection from fungal contamination during storage.

Keywords: silver nanoparticles; poly (methacrylic acid) microspheres; antifungal activity; cultural heritage; food preservation or packaging



Citation: Kainourgios, P.; Tziveleka, L.-A.; Kartsonakis, I.A.; Ioannou, E.; Roussis, V.; Charitidis, C.A. Silver Nanoparticles Grown on Cross-Linked Poly (Methacrylic Acid) Microspheres: Synthesis, Characterization, and Antifungal Activity Evaluation. *Chemosensors* **2021**, *9*, 152. <https://doi.org/10.3390/chemosensors9070152>

Academic Editor: Maria Grzeszczuk

Received: 13 May 2021

Accepted: 19 June 2021

Published: 23 June 2021

Publisher's Note: MDPI stays neutral with regard to jurisdictional claims in published maps and institutional affiliations.



Copyright: © 2021 by the authors. Licensee MDPI, Basel, Switzerland. This article is an open access article distributed under the terms and conditions of the Creative Commons Attribution (CC BY) license (<https://creativecommons.org/licenses/by/4.0/>).

1. Introduction

In recent years, nanotechnology has played a crucial role in food packaging improvement by combining antimicrobial agents with external barrier properties. Food deterioration reduction, resulting in prolonged food preservation, can be feasible through microbial growth retardation or inhibition via nanotechnology usage in packaging products [1,2]. The exploitation and incorporation of nanoparticles with antimicrobial properties into a variety of food contact materials such as papers, spheres, and fibers are a priority for studies aiming at food storage increment [3].

Another field of nanotechnology implementation is related to cultural heritage protection. Most of the tangible cultural heritage is predominantly based on archives (books, maps) and artwork (paintings, drawings, sculptures), usually utilizing paper, wood, or stone [4–6]. These materials are susceptible to degradation and biodeterioration by microorganisms, especially from fungi, since organic matter, like cellulose, is a source of essential nutrients [7]. Fungal growth on stone and wood constitutes a serious challenge as well [8].

Preservation of our heritage aims at conservation with minimal alterations in their pristine physical characteristics. A plethora of strategies have been proposed to effectively address this challenge [9]; most of these approaches focus on biocidal metallic compounds, mainly copper, zinc, and silver. However, these strategies may lack compatibility with the material of the cultural heritage item [10,11] or have a negative environmental impact, such as the bioaccumulation of metals in living organisms [12].

Silver nanoparticles (AgNPs) have attracted significant attention due to their low cytotoxicity towards multicellular organisms, as well as their biocidal properties towards pathogens [13–15]. The mechanism of toxicity of the AgNPs involves the release of silver ions (Ag^+), the generation of reactive oxygen species, and the destruction of the membrane structure [16]. Specifically, Ag^+ is mainly accountable for these toxic properties, either by attaching to thiol groups of biomolecules of microorganisms, creating reactive oxygen species or by interacting with membrane phospholipids and proteins, thus deactivating vital membrane functions [17–20]. Reports on the mechanism of the action of AgNPs on phytopathogens have shown that upon treatment, damage to the surface of fungal hyphae, along with the inhibition of conidial germination are detected [21]. Moreover, the reported microbicidal effect of AgNPs in drug-resistant fungi is achieved through multiple cellular targeting, including fatty acids, important in the hyphal morphogenesis involved in pathogenicity [22]. Furthermore, extensive studies have shown that AgNPs produce silver ions through their oxidation in aqueous biological media, whereas the Ag^+ dissolution rate is highly dependent on the size, morphology, and the capping/stabilizing agent of the AgNPs [23–25]. The majority of the strategies for the chemical synthesis of AgNPs emphasize three main aspects: the silver precursor, the reducing agent, and the stabilizing/capping agent, which grant adequate control over the size distribution of the AgNPs [26]. Nguyen et al. have reported that polyvinylpyrrolidone (PVP) and citrate capped AgNPs exhibited reduced cytotoxicity compared to uncapped AgNPs, whereas AgNPs with diameters of 20–40 nm were 10% more cytotoxic than AgNPs with a diameter of 60–80 nm [27]. Furthermore, Wang et al. have reported higher cytotoxicity for citrate-capped AgNPs compared to PVP-capped AgNPs, whereas increased Ag^+ dissolution was observed for nanoparticles with smaller diameters [28].

Therefore, recent studies propose an alternative approach for the formation of AgNPs to achieve stability and avoid aggregation [29,30]. In these studies, the AgNPs are being formed on functionalized substrates that promote the attachment of Ag^+ (silver precursor) followed by subsequent reduction to form particles [31]. Moreover, the combination of the AgNPs with polymeric substrates has emerged as a promising strategy for the stimuli-triggered release of antimicrobial agents [32]. In this approach, the growth of nanoparticles is not regulated by a capping/stabilizing molecule, but rather by the intermolecular interactions with the substrate and the silver precursor/reducing agent ratio. According to Nguyen et al., nuclei formation is a thermodynamically induced process, therefore space confinement could potentially influence the formation of nanoparticles in terms of size distribution [33]. Carlberg et al. have demonstrated the formation of AgNPs on the surface of functionalized electrospun polyimide fibers in a process labeled as “surface-confined synthesis” that involves either thermal or chemical reduction of the silver ions. According to their findings, the high specific surface area of the electrospun fibers significantly affects the growth of the AgNPs [34]. In the work of Sen et al., an organic–inorganic core–shell microstructure, for the growth of AgNPs on its surface, was synthesized. This strategy utilized electrostatic interactions between the polymers’ carbonyl groups and the silver cations, to initiate particle growth [35]. In addition, Hanish et al. employed functionalized colloidal silica to form AgNPs. It was reported that the functionalization process could promote organized formation on the silica’s surface instead of random growth [36]. According to Levard et al., the exact properties (e.g., surface density, purity) of the capping agent in the AgNPs structure have not been extensively studied, considering the analytical difficulties; consequently, the exact mechanism of how the capping agent affects nanoparticle growth and the nanoparticles’ dissolution rates are currently obscure and difficult to

determine [37]. Evidently, methodologies that employ substrates for the controlled growth of AgNPs without the use of a capping agent could potentially overcome these challenges, while still retaining their antimicrobial efficiency.

Herein, we report the preparation of cross-linked poly (methacrylic acid) (PMAA) microspheres for the growth of AgNPs. PMAA in aqueous media is almost entirely deprotonated and, therefore, can absorb and retain water, and it is accepted as an environmentally friendly chemical structure [38]. Consequently, PMAA is an ideal substrate for the growth of the AgNPs, since it has the potential to significantly contribute to the controlled oxidation of the AgNPs via the absorption of water, while effectively exploiting the association of fungal growth with high moisture levels [39,40]. In addition, the proposed methodology provides an alternative approach for producing stable, uncapped AgNPs. The uncapped surface of AgNPs has the potential to exploit the surface plasmon resonance of AgNPs, thus enabling a variety of sensing applications utilizing the surface-enhanced Raman spectroscopy (SERS) which is closely correlated with the coupling between the electric field of the incident beam and the field stimulated by the collective oscillation of valence electrons [37]. Chatzipavlidis et al. have previously reported the enhanced Raman signal in the detection of the Rhodamine B molecule as a potential imaging application whereas similar SERS methodology has been applied to identify Cr(VI) and organic pollutants, respectively, for environmental analysis applications [40–43]. The proposed methodology for AgNPs synthesis is an alternative to the standard procedure utilizing capping agents for the control over the nanoparticles' size and aggregation whereas it has the potential to provide the foundation for producing nanocomposite materials with tailored properties.

2. Materials and Methods

2.1. Materials and Characterization Methods

Methacrylic acid (MAA), *N-N'*-methylene bis (acrylamide) (MBA), silver nitrate solution (2M), and acetonitrile (ACN) were purchased from Acros Organics. 2,2'-Azobis (isobutyronitrile) (AIBN) and sodium borohydride (NaBH₄) were purchased from Sigma Aldrich. MAA was distilled prior to its use and all other reagents were used as purchased. Tween 80 was obtained from Fischer Scientific (Hampton, NH, USA), while potato dextrose agar (PDA) and potato dextrose broth (PDB) were purchased from Conda (Madrid, Spain).

Infrared spectra (FT-IR) were recorded using a Cary 630 Agilent FTIR spectrometer equipped with a diamond ATR crystal, whereas a 670 UV-Vis spectrophotometer was used to measure the ultraviolet absorption spectra (UV-Vis) of the resulting structures. Scanning and transmittance electron microscopy (SEM, TEM) were employed to determine the size and shape of the synthesized microspheres, and energy dispersive X-ray spectroscopy (EDS) was used for the elemental analysis. The SEM and TEM were accomplished utilizing an FEI inspect microscope with a W (Tungsten) filament operating at 25 kV equipped with EDAX GENESIS (AMETEK PROCESS and ANALYTICAL INSTRUMENTS), and an FEI CM20 microscope operating at 200 kV, respectively. TEM samples were prepared by placing one drop of a diluted sample on a carbon-coated Cu grid and allowing the solvent to evaporate. Thermogravimetric analyses (TGA) were performed on a TGA Netch STA 449 Jupiter, whereas a Malvern Zetasizer Nano ZS apparatus was utilized for measuring the size, polydispersity, and surface charge of the polymer microsphere by dynamic light scattering (DLS).

2.2. Synthesis of P(MAA-co-MBA) Microspheres

For the synthesis of polymer microspheres, a modified version of the distillation precipitation polymerization procedure has been utilized as previously described [44,45]. Briefly, ACN, the monomer methacrylic acid, the cross-linker MBA, and the initiator AIBN were placed in a round-bottom flask and were vigorously stirred under an argon atmosphere. The concentration of the monomer was at 1% *w/v* (in relation to ACN, 350 mL), whereas the concentration of the cross-linker and the initiator were at 10% and 1.25% *w/w*, respectively (in relation to the monomer). After 10 min the mixture turned opalescent and then white, indicating the formation of polymer nanoparticles; at that point, the temperature was in-

creased to 85 °C to initiate the distillation of the solvent and 15 mL of ACN was distilled. Centrifugation at 8000 rpm for 10 min and rinsing with distilled ACN was carried out to remove unreacted species.

2.3. Silver Nanoparticles' Growth on P(MAA-co-MBA) Microspheres (PMAA@Ag)

The growth of AgNPs onto the surface of P(MAA-co-MBA) microspheres was accomplished utilizing the chemical co-precipitation of AgNO₃ in the presence of NaBH₄ as the reducing agent [30]. In a glass beaker 100 mL of deionized water, 100 mg of P(MAA-co-MBA) microspheres, and 50 µL of AgNO₃ (2N) were placed and stirred for varying time periods (1 to 24 h). Prior to the addition of the reducing agent, the colloidal solution was centrifuged (8000 rpm, 10 min) and redispersed in H₂O to remove the free silver ions and the nitrate counter ions. Then, NaBH₄ (10 mM) was added dropwise into the mixture and the color gradually changed from white to yellow, to dark red, and then to light brown, depending on the stirring time of the P(MAA-co-MBA)/AgNO₃ solution, thus indicating the formation of the AgNPs. Figure 1 depicts a schematic representation of the growth of the AgNPs on P(MAA-co-MBA) microspheres (PMAA@Ag).

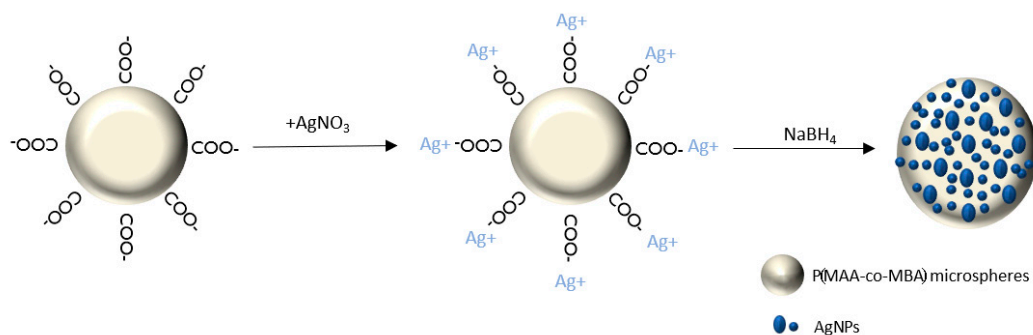


Figure 1. Schematic representation of Ag ion reduction to AgNPs on the surface of P(MAA-co-MBA) microspheres.

2.4. Evaluation of Antifungal Activity Using the Dilution Method

Fungal strain *A. niger* ATCC 16888, used in the antifungal activity evaluation assay, was kindly provided by Dr. Gonou-Zagou (Department of Biology, National and Kapodistrian University of Athens). Fungal spore suspensions were stored in 0.1% Tween and 20% glycerol at −80 °C prior to use. Before each assay, fungal cells were inoculated in PDA plates and grown at 27 °C for four days. Petri dishes (5.5 cm) were covered with PDA culture media in which increasing concentrations of PMAA@Ag in sterile distilled water were added. The selected final concentrations were 5, 1, and 0.5 mg PMAA@Ag/mL. A fungal inoculum (10³ conidia per mL, in 0.1% Triton X-100) was added to each petri dish and the fungal growth was monitored over a positive growth control sample without the addition of any antifungal agent. Plates were incubated at 27 °C and the fungal growth was monitored for up to ten days.

3. Results and Discussion

3.1. Synthesis of PMAA-co-MBA Microspheres

Cross-linking of the polymer microsphere is vital for the spherical shape to be retained in aqueous media. FT-IR spectroscopy was utilized to qualitatively identify the cross-linking of the P(MAA-co-MBA) microspheres. Therefore, an additional sample of PMAA microspheres was prepared under the same conditions in the absence of the crosslinker. As shown in Figure 2, it can be observed that the spectra of both materials exhibit a strong vibration at approximately 1700 cm^{−1} which is attributed to the carbonyl vibration, yet the IR spectrum of P(MAA-co-MBA) exhibits an additional peak at 1531 cm^{−1}, corresponding to the amide vibration of the cross-linker's molecule. Evidently, the two spectra exhibit identical vibrations with the exception of the vibration at 1531 cm^{−1} at the P(MAA-co-MBA) spectrum which

corresponds to the amide bond vibration evidencing qualitatively the successful cross-linking of the PMAA polymer.

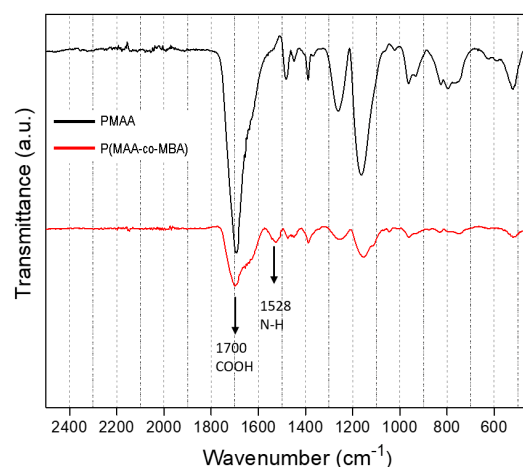


Figure 2. FT-IR spectra of PMAA and P(MAA-co-MBA) microspheres.

3.2. Size Distribution and Surface Charge of the P(MAA-co-MBA) Microspheres

Microspheres of P(MAA-co-MBA) serve as substrates for the growth of the AgNPs, consequently, the size distribution, as well as the surface charge, have a close relationship with the nucleation and growth of the AgNPs. Figure 3 illustrates the results obtained from the DLS measurements of the polymerized P(MAA-co-MBA) microspheres dispersed in H₂O prior to the growth of the AgNPs. Figure 3a reveals that the hydrodynamic radius of the microspheres in H₂O is at 419 ± 109 nm, whereas the polydispersity index obtained by the correlation coefficient diagram (Figure 3b) is at 0.062, indicating monodisperse microspheres. Evidently, the resulting microspheres have a very narrow size distribution, which was further supported by SEM microscopy (Figure 4a), where the actual microsphere diameter is measured approximately at 200 ± 15 nm, whereas ζ -potential measurements affirm that the microspheres possess a strongly negative surface charge at -50 ± 5.34 mV, as illustrated in Figure 3c. Figure 4b presents the results of the EDS elemental analysis after the growth of the AgNPs. A broad excitation peak can be seen at 2.9 KeV which is attributed to metallic silver (15.22%), whereas Ag₂O or hybrid Ag/Ag₂O are absent. According to the literature, these species are expected to exert smaller energies, around 0–1.35 KeV [46]. Carbon and oxygen peaks are attributed to the organic polymer counterpart, whereas gold was identified due to the sampling process for SEM analysis. Although elemental quantification of silver in EDS analysis was indicative, the results (15.22%) do not differ considerably when compared to the quantification analysis derived from TGA (23%); these differences could be attributed to the presence of Au in the EDS analysis.

3.3. Growth of AgNPs

It has been shown that increasing AgNO₃ concentration promotes both nucleation and growth of AgNPs [47]. In the current study, the Coulomb interaction between silver ions and the carboxyl-terminal groups of the polymer's chain was selected as the driving force for the initiation of nanoparticle growth instead of the initial AgNO₃ concentration. Therefore, during the stirring of the microspheres with AgNO₃, aliquots were sampled every hour for 7 h, and a final sample was collected after 24 h of stirring. Each sample was centrifuged to remove nitrates and free silver ions, subsequently redispersed in the initial sample volume and finally reduced to AgNPs using 10 mM NaBH₄. Each aliquot was measured in a UV-Vis spectrophotometer. Figure 5a depicts the UV spectra of the analyzed samples. The absorption peak shifted in different wavenumbers, yet a constant correlation between stirring time and peak shift was not observed. Table 1 shows the absorption band wavenumber, full width at half maximum (FWHM), and band area in correlation with stirring time. The FWHM, as well as the area of each band, were gradually increasing up

to 5 h of stirring; from there on, a shift to the initial values was observed. This time effect can be observed in Figure 5b, where vials containing the corresponding aliquots after the Ag^+ reduction to AgNPs with NaBH_4 are illustrated. Specifically, after 24 h of stirring, the color tends to return to the initial shade acquired within the first hour of stirring.

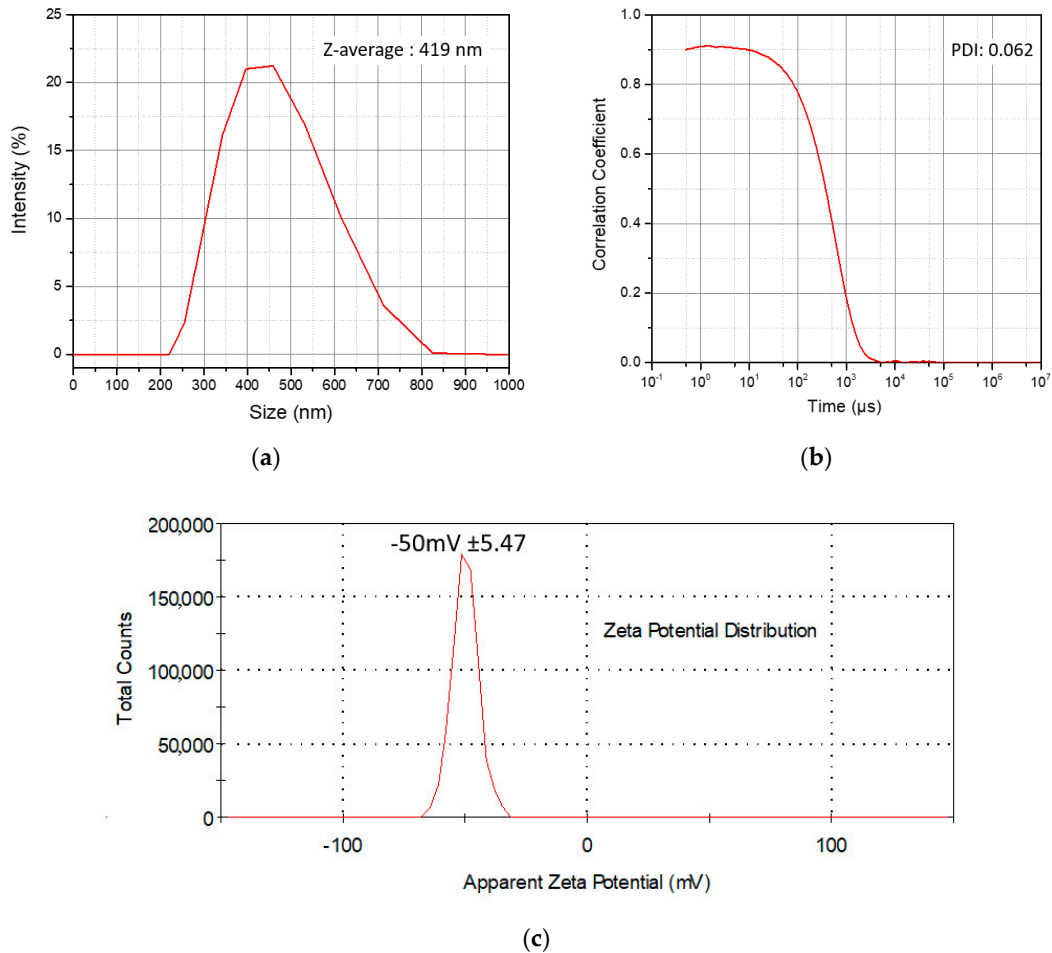


Figure 3. DLS measurements of the PMAA-co-MBA microspheres (a) average hydrodynamic radius size distribution; (b) correlation function diagram; (c) ζ -potential-surface charge distribution.

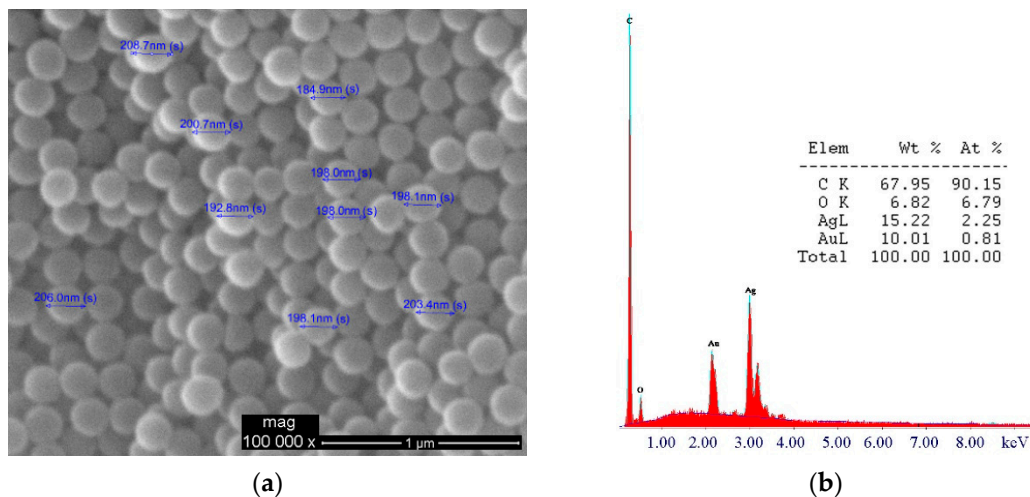


Figure 4. (a) SEM image of the P(MAA-co-MBA) microspheres; (b) EDS analysis of the PMAA@Ag structures.

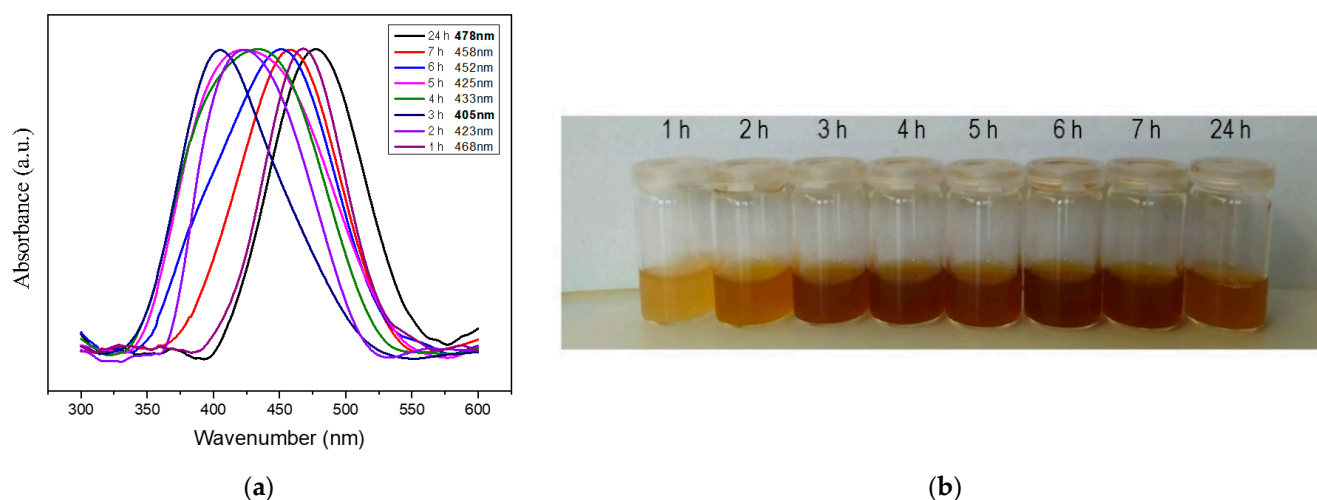


Figure 5. (a) UV absorption spectra of the PMAA@Ag aliquots sampled at different time periods; (b) vials containing the PMAA@Ag aliquots after reduction with NaBH_4 .

Table 1. Absorption band maxima, FWHM, and area versus time of stirring in AgNO_3 .

Time of Stirring in AgNO_3 (h)	Absorption Band Maximum (nm)	Band FWHM	Band Area
1	468	68.53	10.52
2	423	84.97	13.14
3	405	88.98	13.53
4	433	110.38	18.73
5	425	116.13	19.75
6	452	103.90	16.24
7	458	84.89	13.15
24	478	78.19	12.23

According to Hegde et al., AgNPs (<10 nm) with a spherical shape exhibit an absorption band with a maximum of 400 nm [48], whereas nanoparticle aggregation shifts the band to higher wavenumbers [49]. Furthermore, Garcia et al. showed the influence of the increased particle size distribution of AgNPs in the broadening of the absorption band. In particular, AgNPs with the same average size but wider size distributions exhibited broader FWHM in their absorption bands [50]. From the above results and observations, it is safe to deduce that the mechanism of electrostatic attachment of Ag^+ to the polymeric microspheres is of a dynamic nature. Therefore, 3 h of P(MAA-co-MBA) stirring microspheres in AgNO_3 solution was chosen as the optimum condition to proceed for further characterization, as well as antifungal activity assessment, since the absorption band is at 403 nm and the FWHM is at the average measured value, indicating the presence of spherical AgNPs with an average size distribution, respectively. Moreover, the FWHM to band area ratio (Table 1) shows that after 3 h of stirring, minimum particle aggregation is achieved.

To correlate these results with the average size of the AgNPs, TEM analysis was conducted, and the results are presented in Figure 6. In Figure 6a (scale bar at 500 nm) large (~20 nm) spherical AgNPs are observed on the surface of the polymeric microspheres, whereas on the top right of the image a cluster of spherical nanoparticles can be seen, supporting the aggregation of AgNPs. At larger magnifications (Figure 6b–d), spherical AgNPs of a smaller diameter (<10 nm) are mostly observed, yet with large size distributions, thus further supporting the results obtained via the UV-Vis absorption spectra in terms of band area and band absorption maximum. Nevertheless, detached AgNPs can also be seen orbiting the P(MAA-co-MBA) surface in almost all images of Figure 6. This phenomenon is probably the result of the electron beam affecting the electrostatically attached AgNPs; a similar phenomenon was observed for gold nanoparticles according to Chen et al. in an attempt to manipulate gold nanoparticles utilizing an electron beam [51].

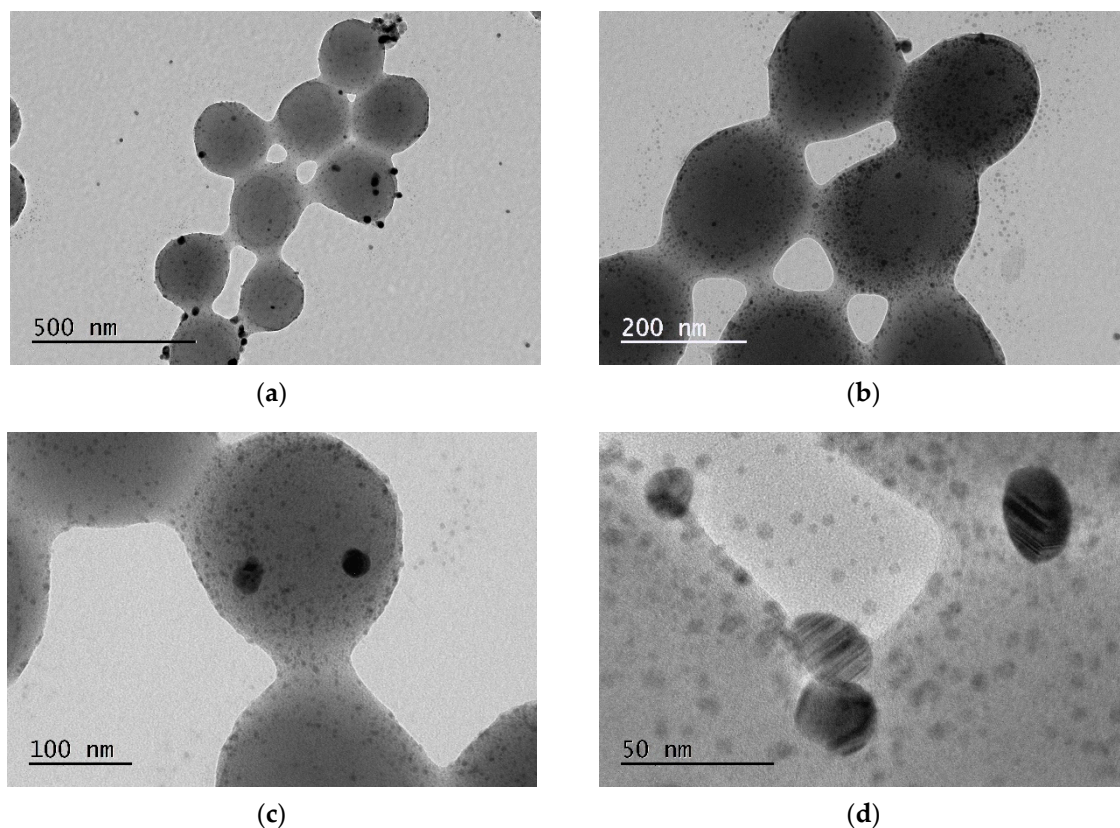


Figure 6. (a–d) TEM images of the PMAA@Ag sample (3 h stirring in AgNO₃) under different magnifications.

3.4. Quantification of AgNPs

The mass percentage quantification of the AgNPs in the resulting composite nanostructure was accomplished via TGA. Figure 7a exhibits the TGA curve for the P(MAA-co-MBA) sample prior to the AgNPs growth (black curve), whereas the red curve represents the TGA curve after the growth of the nanoparticles (PMAA@Ag). The pristine PMAA-co-MBA has a residual mass of 11%, whereas the composite nanostructure exhibits a residual mass of 22%. Both curves start their thermal degradation at 318 °C and reach a plateau in terms of thermal degradation, at 450 °C and 423 °C for the PMAA-co-MBA and PMAA@Ag, respectively. According to Cárdenas et al. [52], the homopolymer PMAA exhibits a thermal degradation temperature at approximately 400 °C with minor deviations due to molecular weight differences. The 22% residual mass generated by the PMAA@Ag sample is the sum of the residual polymer (11% according to the black curve) and the residual Ag (11%). AgNPs are known to exhibit increased thermal conductivity; in our measurement, this can be observed by the rapid thermal degradation of the PMAA@Ag sample compared to the pristine PMAA sample. In addition, Hausner et al. [53], while studying the thermal decomposition of capped AgNPs observed that uncapped AgNPs of average size distribution of 6 nm start to sinter at 400 °C. In the present study, TEM analysis has confirmed the presence of AgNPs with sizing of 5–6 nm (Figure 6b–d). The two materials, PMAA-co-MBA and AgNPs, exhibit similar thermal degradation. As such, the mass percentage of the PMAA@Ag sample was subtracted from the mass percentage of the PMAA-co-MBA sample and was then plotted vs. temperature. These results are observed in Figure 7b. A similar method was applied by Kunc et al. for the quantification of silica amide functional groups utilizing TGA and NMR [54]. Indeed, at approximately 398 °C, a 12% mass increase can be observed for the PMAA@Ag sample which is attributed to the thermal degradation of smaller diameter (~6 nm) AgNPs. Therefore, the AgNPs percentage in the PMAA@Ag structure was estimated as 23% (11% residual and 12% thermally degraded at 398 °C).

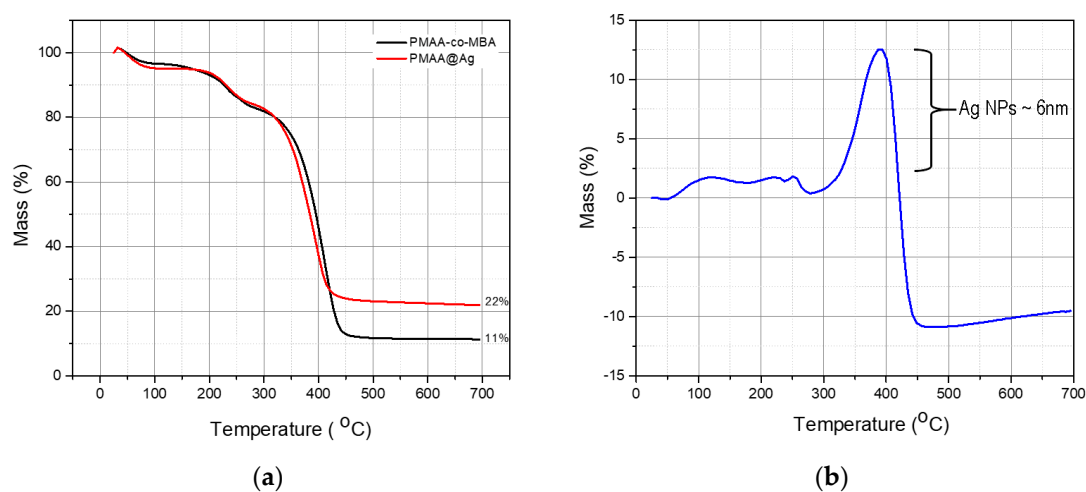


Figure 7. (a) TGA curves for the PMAA-co-MBA and the PMAA@Ag sample; (b) mass percentage subtraction [(PMAA-co-MBA%—PMAA@Ag%)] of the curves presented in Figure 7a vs. temperature.

3.5. Antifungal Activity Assessment

For the antifungal activity evaluation, petri dishes were covered with a PDA layer loaded with increasing concentrations of PMAA@Ag nanostructures (0.5, 1, and 5 mg/mL) and incubated at their optimum growth conditions for up to ten days. As observed in Figure 8, after 48 h of incubation, fungal growth was clearly visible in the control samples, while no growth was observed in plates treated with PMAA@Ag at all concentrations examined. *A. niger* began to proliferate on the PMAA@Ag-treated agar on the 4th and 7th day of incubation, when the lower concentrations of 0.5 and 1 mg PMAA@Ag/mL, respectively, were employed. However, when 5 mg PMAA@Ag/mL solution, corresponding to approximately 1 mg AgNPs/mL, was used, the growth of *A. niger* was completely inhibited even after longer incubation times of up to ten days. Hence, PMAA@Ag nanostructures exhibit fungicidal activity at a concentration equal to 5 mg/mL, while at lower concentrations only fungistatic activity is observed.

Although the biocidal effect and mode of action of AgNPs have long been known [55], their antifungal activity mechanism has only recently been elucidated. *Candida albicans* cells were employed for the clarification of the antifungal mode of action of AgNPs [56]. During exposure of *C. albicans* to AgNPs, significant changes to the fungal membranes were observed, resulting in the formation of pores, and, finally, cell death. The possible mechanism by which the AgNPs break down the membrane permeability barrier is by perturbing the membrane lipid bilayers, causing the leakage of ions and other materials, as well as forming pores and dissipating the electrical potential of the membrane.

AgNPs usually range in size from 1–200 nm, and as the particle size decreases, the surface area to volume ratio greatly increases. Consequently, the physicochemical, and especially the biological properties, of AgNPs are markedly improved as compared to the original material. Although AgNPs sizing from 1–10 nm are known to exert the highest antimicrobial activity [57,58] even at low concentrations, previous studies on fungi have shown that, in some cases, high concentrations of metallic NPs are needed for the antifungal activity to be exerted [4–6,59]. These interactions and their effect on membrane integrity are directly dependent on the size, the shape, and the AgNPs concentration. Apart from depending on the concentration of the AgNPs, the extent of inhibition also depends on the initial microbial population [60]. Specifically, Levard et al. [37] reported on these particles' interactions with intracellular substances from lysed cells, causing, therefore, their coagulation and the particles' exclusion from the liquid system.

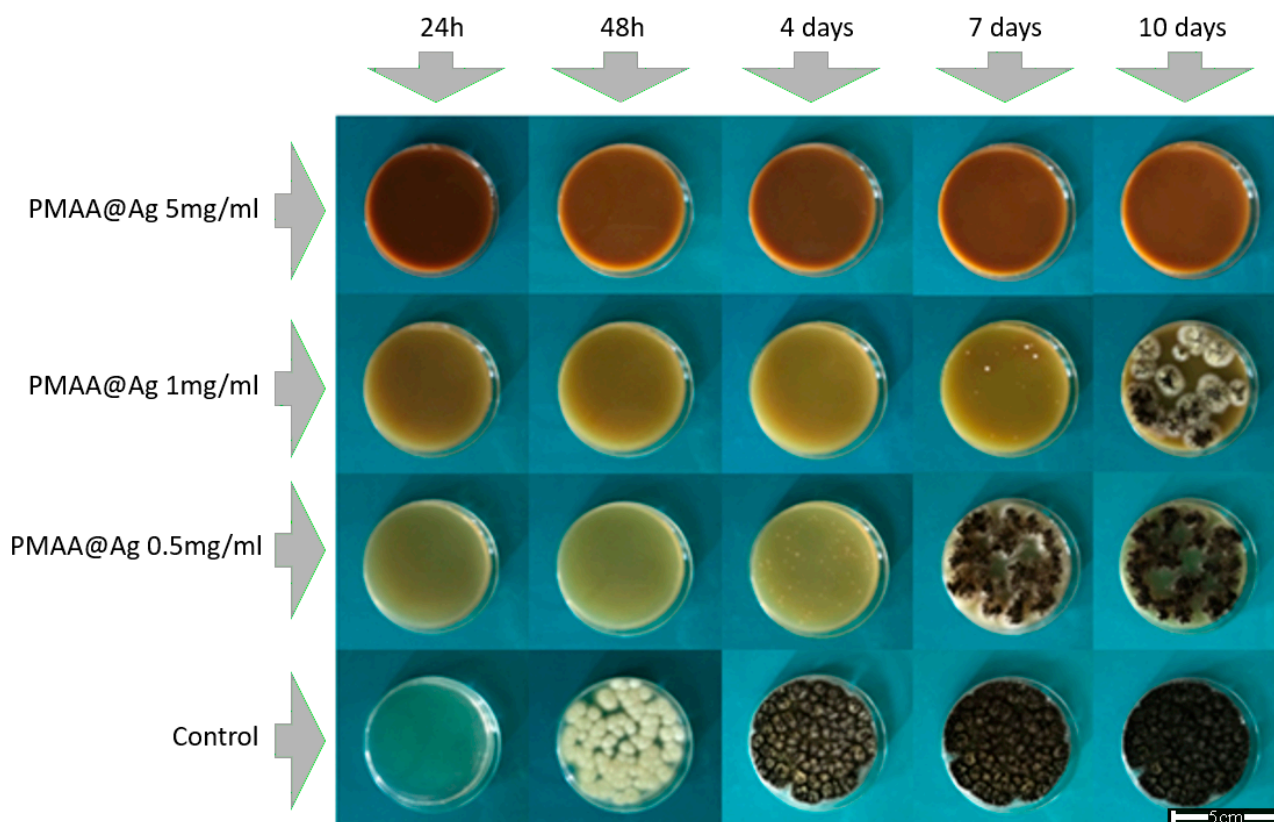


Figure 8. Antifungal activity exerted by different concentrations of PMAA@Ag (5 mg/mL, 1 mg/mL, 0.5 mg/mL) against *Aspergillus niger* after 24 h, 48 h, 4 days, 7 days, and 10 days of incubation.

4. Conclusions

Cross-linked poly (methacrylic acid) microspheres have been successfully prepared by utilizing the distillation precipitation method. Coulomb forces between silver cations and polymeric carboxyl side groups were employed as the driving force to promote the growth of silver nanoparticles on the surface of the P(MAA-co-MBA) microspheres, whereas UV-Vis and TEM microscopy revealed that these electrostatic interactions are of a dynamic nature. Our results evidenced that a 3 h stirring of P(MAA-co-MBA) microspheres in AgNO_3 was the appropriate time for the growth of AgNPs with an average size polydispersity. These results further suggest that the proposed methodology could result in nanostructures with tunable size and consequently, properties. The antifungal assessment against the growth of *A. niger* showed a fungistatic action in lower concentrations, whereas at higher concentrations the PMAA@Ag nanostructures exhibited fungicidal activity. The produced materials can be used for antifungal applications such as additives in filters, membranes, and storage packages in the medical, food, and cultural heritage (preventive conservation) sectors. However, it should be mentioned that, regarding food packages, AgNPs migration tests should be carried out; our future plans include the performance of these tests together with the evaluation of the antifungal activity of the obtained materials with respect to other fungi.

Author Contributions: Conceptualization, P.K., and C.A.C.; methodology, P.K. and L.-A.T.; software, P.K.; validation, P.K., L.-A.T. and C.A.C.; formal analysis, P.K., L.-A.T. and I.A.K.; investigation, P.K. and L.-A.T.; resources, P.K., I.A.K., E.I. and V.R.; data curation, P.K.; writing—original draft preparation, P.K., L.-A.T. and I.A.K.; writing—review and editing, E.I., V.R. and C.A.C.; visualization, P.K. and L.-A.T.; supervision, C.A.C.; project administration, C.A.C.; funding acquisition, C.A.C. All authors have read and agreed to the published version of the manuscript.

Funding: This research was funded by the European Union’s HORIZON 2020 research and innovation program, grant agreement no. 814496 (APACHE).

Institutional Review Board Statement: Not applicable.

Informed Consent Statement: Not applicable.

Data Availability Statement: Data sharing not applicable.

Conflicts of Interest: The authors declare no conflict of interest.

References

1. Braga, L.R.; Rangel, E.T.; Suarez, P.A.Z.; Machado, F. Simple synthesis of active films based on PVC incorporated with silver nanoparticles: Evaluation of the thermal, structural and antimicrobial properties. *Food Packag. Shelf Life* **2018**, *15*, 122–129. [[CrossRef](#)]
2. Kumar, S.; Basumatary, I.B.; Sudhani, H.P.K.; Bajpai, V.K.; Chen, L.; Shukla, S.; Mukherjee, A. Plant extract mediated silver nanoparticles and their applications as antimicrobials and in sustainable food packaging: A state-of-the-art review. *Trends Food Sci. Technol.* **2021**, *112*, 651–666. [[CrossRef](#)]
3. Zhao, X.; Wang, K.; Ai, C.; Yan, L.; Jiang, C.; Shi, J. Improvement of antifungal and antibacterial activities of food packages using silver nanoparticles synthesized by iturin A. *Food Packag. Shelf Life* **2021**, *28*, 100669. [[CrossRef](#)]
4. Silva, M.; Rosado, T.; Gonzalez-Pérez, M.; Gobbo, D.; Teixeira, D.; Candeias, A.; Caldeira, A.T. Production of Antagonistic Compounds by *Bacillus* sp. with Antifungal Activity against Heritage Contaminating Fungi. *Coatings* **2018**, *8*, 123. [[CrossRef](#)]
5. Goffredo, G.B.; Citterio, B.; Biavasco, F.; Stazi, F.; Barcelli, S.; Munafò, P. Nanotechnology on wood: The effect of photocatalytic nanocoatings against *Aspergillus niger*. *J. Cult. Herit.* **2017**, *27*, 125–136. [[CrossRef](#)]
6. Castillo, I.F.; Guillén, E.G.; Jesús, M.; Silva, F.; Mitchell, S.G. Preventing fungal growth on heritage paper with antifungal and cellulase inhibiting magnesium oxide nanoparticles. *J. Mater. Chem. B* **2019**, *7*, 6412–6419. [[CrossRef](#)]
7. Treseder, K.K.; Lennon, J.T. Fungal Traits That Drive Ecosystem Dynamics on Land. *Microbiol. Mol. Biol. Rev.* **2015**, *79*, 243. [[CrossRef](#)]
8. McNamara, C.J.; Mitchell, R. Microbial deterioration of historic stone. *Front. Ecol. Environ.* **2005**, *3*, 445–451. [[CrossRef](#)]
9. Flemming, H.C. Alternative and conventional anti-fouling strategies. *Int. Biodeterior. Biodegrad.* **2005**, *56*, 121–134. [[CrossRef](#)]
10. Shabir Mahr, M.; Hübert, T.; Stephan, I.; Miltz, H. Decay protection of wood against brown-rot fungi by titanium alkoxide impregnations. *Int. Biodeterior. Biodegrad.* **2013**, *77*, 56–62. [[CrossRef](#)]
11. Unger, A. Decontamination and “deconsolidation” of historical wood preservatives and wood consolidants in cultural heritage. *J. Cult. Herit.* **2012**, *13*, S196–S202. [[CrossRef](#)]
12. Khan, M.I.; Khisroon, M.; Khan, A.; Gulfam, N.; Siraj, M.; Zaidi, F.; Ahmadullah; Abidullah; Fatima, S.H.; Noreen, S.; et al. Bioaccumulation of Heavy Metals in Water, Sediments, and Tissues and Their Histopathological Effects on *Anodonta cygnea* (Linea, 1876) in Kabul River, Khyber Pakhtunkhwa, Pakistan. *BioMed. Res. Int.* **2018**, *2018*, 1910274. [[CrossRef](#)]
13. Pryshchepa, O.; Pomastowski, P.; Buszewski, B. Silver nanoparticles: Synthesis, investigation techniques, and properties. *Adv. Colloid Interface Sci.* **2020**, *284*, 102246. [[CrossRef](#)] [[PubMed](#)]
14. Takamiya, A.S.; Monteiro, D.R.; Gorup, L.F.; Silva, E.A.; de Camargo, E.R.; Gomes-Filho, J.E.; de Oliveira, S.H.P.; Barbosa, D.B. Biocompatible silver nanoparticles incorporated in acrylic resin for dental application inhibit *Candida albicans* biofilm. *Mater. Sci. Eng. C* **2021**, *118*, 111341. [[CrossRef](#)] [[PubMed](#)]
15. Craciunescu, O.; Seciu, A.-M.; Zarnescu, O. In vitro and in vivo evaluation of a biomimetic scaffold embedding silver nanoparticles for improved treatment of oral lesions. *Mater. Sci. Eng. C* **2021**, *123*, 112015. [[CrossRef](#)] [[PubMed](#)]
16. Xu, L.; Wang, Y.Y.; Huang, J.; Chen, C.Y.; Wang, Z.X.; Xie, H. Silver nanoparticles: Synthesis, medical applications and biosafety. *Theranostics* **2020**, *10*, 8996–9031. [[CrossRef](#)] [[PubMed](#)]
17. Dibrov, P.; Dzioba, J.; Gosink, K.K.; Häse, C.C. Chemiosmotic Mechanism of Antimicrobial Activity of Ag⁺ in *Vibrio cholerae*. *Antimicrob. Agents Chemother.* **2002**, *46*, 2668. [[CrossRef](#)]
18. Park, H.-J.; Kim, J.Y.; Kim, J.; Lee, J.-H.; Hahn, J.-S.; Gu, M.B.; Yoon, J. Silver-ion-mediated reactive oxygen species generation affecting bactericidal activity. *Water Res.* **2009**, *43*, 1027–1032. [[CrossRef](#)] [[PubMed](#)]
19. Gordon, O.; Vig Slenters, T.; Brunetto, P.S.; Villaruz, A.E.; Sturdevant, D.E.; Otto, M.; Landmann, R.; Fromm, K.M. Silver Coordination Polymers for Prevention of Implant Infection: Thiol Interaction, Impact on Respiratory Chain Enzymes, and Hydroxyl Radical Induction. *Antimicrob. Agents Chemother.* **2010**, *54*, 4208. [[CrossRef](#)] [[PubMed](#)]
20. Beer, C.; Foldbjerg, R.; Hayashi, Y.; Sutherland, D.S.; Autrup, H. Toxicity of silver nanoparticles—Nanoparticle or silver ion? *Toxicol. Lett.* **2012**, *208*, 286–292. [[CrossRef](#)]
21. Kim, S.W.; Kim, K.S.; Lamsal, K.; Kim, Y.J.; Kim, S.B.; Jung, M.; Sim, S.J.; Kim, H.S.; Chang, S.J.; Kim, J.K.; et al. An in vitro study of the antifungal effect of silver nanoparticles on oak wilt pathogen *Raffaella* sp. *J. Microbiol. Biotechnol.* **2009**, *19*, 760–764. [[PubMed](#)]
22. Radhakrishnan, V.S.; Mudiam, M.K.R.; Kumar, M.; Dwivedi, S.P.; Singh, S.P.; Prasad, T. Silver nanoparticles induced alterations in multiple cellular targets, which are critical for drug susceptibilities and pathogenicity in fungal pathogen (*Candida albicans*). *Int. J. Nanomed.* **2018**, *13*, 2647–2663. [[CrossRef](#)] [[PubMed](#)]

23. Ivask, A.; Kurvet, I.; Kasemets, K.; Blinova, I.; Aruoja, V.; Suppi, S.; Vija, H.; Käkinen, A.; Titma, T.; Heinlaan, M.; et al. Size-Dependent Toxicity of Silver Nanoparticles to Bacteria, Yeast, Algae, Crustaceans and Mammalian Cells In Vitro. *PLoS ONE* **2014**, *9*, e102108. [[CrossRef](#)] [[PubMed](#)]
24. Kittler, S.; Greulich, C.; Diendorf, J.; Köller, M.; Epple, M. Toxicity of Silver Nanoparticles Increases during Storage Because of Slow Dissolution under Release of Silver Ions. *Chem. Mater.* **2010**, *22*, 4548–4554. [[CrossRef](#)]
25. Dorobantu, L.S.; Fallone, C.; Noble, A.J.; Veinot, J.; Ma, G.; Goss, G.G.; Burrell, R.E. Toxicity of silver nanoparticles against bacteria, yeast, and algae. *J. Nanopart. Res.* **2015**, *17*, 172. [[CrossRef](#)]
26. Akter, M.; Sikder, M.T.; Rahman, M.M.; Ullah, A.K.M.A.; Hossain, K.F.B.; Banik, S.; Hosokawa, T.; Saito, T.; Kurasaki, M. A systematic review on silver nanoparticles-induced cytotoxicity: Physicochemical properties and perspectives. *J. Adv. Res.* **2018**, *9*, 1–16. [[CrossRef](#)]
27. Nguyen, K.C.; Seligy, V.L.; Massarsky, A.; Moon, T.W.; Rippstein, P.; Tan, J.; Tayabali, A.F. Comparison of toxicity of uncoated and coated silver nanoparticles. *J. Phys. Conf. Ser.* **2013**, *429*, 012025. [[CrossRef](#)]
28. Wang, X.; Ji, Z.; Chang, C.H.; Zhang, H.; Wang, M.; Liao, Y.-P.; Lin, S.; Meng, H.; Li, R.; Sun, B.; et al. Use of Coated Silver Nanoparticles to Understand the Relationship of Particle Dissolution and Bioavailability to Cell and Lung Toxicological Potential. *Small* **2014**, *10*, 385–398. [[CrossRef](#)]
29. Hamouda, H.I.; Abdel-Ghafar, H.M.; Mahmoud, M.H.H. Multi-walled carbon nanotubes decorated with silver nanoparticles for antimicrobial applications. *J. Environ. Chem. Eng.* **2021**, *9*, 105034. [[CrossRef](#)]
30. Ngoc Dung, T.T.; Phan Thi, L.-A.; Nam, V.N.; Nhan, T.T.; Quang, D.V. Preparation of silver nanoparticle-containing ceramic filter by in-situ reduction and application for water disinfection. *J. Environ. Chem. Eng.* **2019**, *7*, 103176. [[CrossRef](#)]
31. Wang, Q.; Barnes, L.-M.; Maslakov, K.I.; Howell, C.A.; Illsley, M.J.; Dyer, P.; Savina, I.N. In situ synthesis of silver or selenium nanoparticles on cationized cellulose fabrics for antimicrobial application. *Mater. Sci. Eng. C* **2021**, *121*, 111859. [[CrossRef](#)]
32. Moorcroft, S.C.T.; Jayne, D.G.; Evans, S.D.; Ong, Z.Y. Stimuli-Responsive Release of Antimicrobials Using Hybrid Inorganic Nanoparticle-Associated Drug-Delivery Systems. *Macromol. Biosci.* **2018**, *18*, e1800207. [[CrossRef](#)]
33. Thanh, N.T.K.; Maclean, N.; Mahiddine, S. Mechanisms of Nucleation and Growth of Nanoparticles in Solution. *Chem. Rev.* **2014**, *114*, 7610–7630. [[CrossRef](#)]
34. Carlberg, B.; Ye, L.-L.; Liu, J. Surface-Confined Synthesis of Silver Nanoparticle Composite Coating on Electrospun Polyimide Nanofibers. *Small* **2011**, *7*, 3057–3066. [[CrossRef](#)] [[PubMed](#)]
35. Yan, S.; Jiang, C.; Guo, J.; Fan, Y.; Zhang, Y. Synthesis of Silver Nanoparticles Loaded onto Polymer-Inorganic Composite Materials and Their Regulated Catalytic Activity. *Polymers* **2019**, *11*, 401. [[CrossRef](#)]
36. Hanisch, M.; Mačković, M.; Taccardi, N.; Spiecker, E.; Klupp Taylor, R.N. Synthesis of silver nanoparticle necklaces without explicit addition of reducing or templating agents. *Chem. Commun.* **2012**, *48*, 4287–4289. [[CrossRef](#)] [[PubMed](#)]
37. Levard, C.; Hotze, E.M.; Lowry, G.V.; Brown, G.E., Jr. Environmental transformations of silver nanoparticles: Impact on stability and toxicity. *Environ. Sci. Technol.* **2012**, *46*, 6900–6914. [[CrossRef](#)] [[PubMed](#)]
38. Kaur, K.; Jindal, R.; Saini, D. Synthesis, optimization and characterization of PVA-co-poly(methacrylic acid) green adsorbents and applications in environmental remediation. *Polym. Bull.* **2020**, *77*, 3079–3100. [[CrossRef](#)]
39. Chen, F.; Yang, X.; Wu, Q. Antifungal capability of TiO₂ coated film on moist wood. *Build. Environ.* **2009**, *44*, 1088–1093. [[CrossRef](#)]
40. Chatzipavlidis, A.; Bilalis, P.; Tziveleka, L.A.; Boukos, N.; Charitidis, C.A.; Kordas, G. Nanostructuring the surface of dual responsive hollow polymer microspheres for versatile utilization in nanomedicine-related applications. *Langmuir* **2013**, *29*, 9562–9572. [[CrossRef](#)]
41. Kneipp, K.; Moskovits, M.; Kneipp, H. *Surface-Enhanced Raman Scattering—Physics and Applications*; Springer: Berlin/Heidelberg, Germany, 2006; ISBN 978-3-540-33567-2.
42. Du, J.; Jing, C. Preparation of Fe₃O₄@Ag SERS substrate and its application in environmental Cr(VI) analysis. *J. Colloid Interface Sci.* **2011**, *358*, 54–61. [[CrossRef](#)] [[PubMed](#)]
43. An, Q.; Zhang, P.; Li, J.M.; Ma, W.F.; Guo, J.; Hu, J.; Wang, C.C. Silver-coated magnetite-carbon core-shell microspheres as substrate-enhanced SERS probes for detection of trace persistent organic pollutants. *Nanoscale* **2012**, *4*, 5210–5216. [[CrossRef](#)]
44. Bai, F.; Huang, B.; Yang, X.; Huang, W. Synthesis of monodisperse poly(methacrylic acid) microspheres by distillation-precipitation polymerization. *Eur. Polym. J.* **2007**, *43*, 3923–3932. [[CrossRef](#)]
45. Bilalis, P.; Boukos, N.; Kordas, G.C. Novel PEGylated pH-sensitive polymeric hollow microspheres. *Mater. Lett.* **2012**, *67*, 180–183. [[CrossRef](#)]
46. Khan, S.B.; Rahman, M.M.; Marwani, H.M.; Asiri, A.M.; Alamry, K.A. Exploration of silver oxide nanoparticles as a pointer of lanthanum for environmental applications. *J. Taiwan Inst. Chem. Eng.* **2014**, *45*, 2770–2776. [[CrossRef](#)]
47. Ma, Z.; Liu, J.; Liu, Y.; Zheng, X.; Tang, K. Green synthesis of silver nanoparticles using soluble soybean polysaccharide and their application in antibacterial coatings. *Int. J. Biol. Macromol.* **2021**, *166*, 567–577. [[CrossRef](#)]
48. Hegde, H.; Santhosh, C.; Sinha, R.K. Seed mediated synthesis of highly stable CTAB capped triangular silver nanoplates for LSPR sensing. *Mater. Res. Express* **2019**, *6*, 105075. [[CrossRef](#)]
49. Huang, T.; Xu, X.-H.N. Synthesis and characterization of tunable rainbow colored colloidal silver nanoparticles using single-nanoparticle plasmonic microscopy and spectroscopy. *J. Mater. Chem.* **2010**, *20*, 9867–9876. [[CrossRef](#)]
50. Garcia, M.A. Surface plasmons in metallic nanoparticles: Fundamentals and applications. *J. Phys. D Appl. Phys.* **2011**, *44*, 283001. [[CrossRef](#)]

51. Chen, Y.-T.; Wang, C.-Y.; Hong, Y.-J.; Kang, Y.-T.; Lai, S.-E.; Chang, P.; Yew, T.-R. Electron beam manipulation of gold nanoparticles external to the beam. *RSC Adv.* **2014**, *4*, 31652–31656. [[CrossRef](#)]
52. Cárdenas, G.; Muñoz, C.; Carbacho, H. Thermal properties and TGA–FTIR studies of polyacrylic and polymethacrylic acid doped with metal clusters. *Eur. Polym. J.* **2000**, *36*, 1091–1099. [[CrossRef](#)]
53. Hausner, S.; Weis, S.; Wielage, B.; Wagner, G. Low temperature joining of copper by Ag nanopaste: Correlation of mechanical properties and process parameters. *Weld. World* **2016**, *60*, 1277–1286. [[CrossRef](#)]
54. Kunc, F.; Balhara, V.; Sun, Y.; Daroszewska, M.; Jakubek, Z.J.; Hill, M.; Brinkmann, A.; Johnston, L.J. Quantification of surface functional groups on silica nanoparticles: Comparison of thermogravimetric analysis and quantitative NMR. *Analyst* **2019**, *144*, 5589–5599. [[CrossRef](#)] [[PubMed](#)]
55. Marambio-Jones, C.; Hoek, E.M.V. A review of the antibacterial effects of silver nanomaterials and potential implications for human health and the environment. *J. Nanopart. Res.* **2010**, *12*, 1531–1551. [[CrossRef](#)]
56. Kim, K.-J.; Sung, W.S.; Suh, B.K.; Moon, S.-K.; Choi, J.-S.; Kim, J.G.; Lee, D.G. Antifungal activity and mode of action of silver nano-particles on *Candida albicans*. *BioMetals* **2009**, *22*, 235–242. [[CrossRef](#)] [[PubMed](#)]
57. Lara, H.H.; Garza-Treviño, E.N.; Ixtepan-Turrent, L.; Singh, D.K. Silver nanoparticles are broad-spectrum bactericidal and virucidal compounds. *J. Nanobiotechnol.* **2011**, *9*, 30. [[CrossRef](#)]
58. Morones, J.R.; Elechiguerra, J.L.; Camacho, A.; Holt, K.; Kouri, J.B.; Ramírez, J.T.; Yacaman, M.J. The bactericidal effect of silver nanoparticles. *Nanotechnology* **2005**, *16*, 2346–2353. [[CrossRef](#)]
59. Ansari, M.A.; Asiri, S.M.M.; Alzohairy, M.A.; Alomary, M.N.; Almatroudi, A.; Khan, F.A. Biofabricated Fatty Acids-Capped Silver Nanoparticles as Potential Antibacterial, Antifungal, Antibiofilm and Anticancer Agents. *Pharmaceuticals* **2021**, *14*, 139. [[CrossRef](#)]
60. Khatoun, U.T.; Rao, G.V.S.N.; Mohan, M.K.; Ramanaviciene, A.; Ramanavicius, A. Comparative study of antifungal activity of silver and gold nanoparticles synthesized by facile chemical approach. *J. Environ. Chem. Eng.* **2018**, *6*, 5837–5844. [[CrossRef](#)]